

Chapter 2

Low-Cost IR Visualizer Based on a Rotating Phosphor Screen for Accurate Beam Analysis

Jaebin Chang, Jangbeom Lee and Suchei Moon

Abstract We present a low-cost IR beam analysis tool based on a rotating phosphor screen. The infrared light incident on the IR-sensitive screen was converted to visible light by the IR-responsive phosphor that operated by light charging and IR-induced luminescence. Through comparative experiments, the conventional IR viewing card, based on the same kind of phosphor, was found to exhibit a short luminescence time because the excited fluorescent molecules are depleted locally at the beam spot. This effect hinders accurate estimation on the spatial characteristic of the IR beam and consequently limits the capability of the IR viewing card in beam inspection. Our IR visualizer alleviates this effect by rotating the IR-sensitive screen in a high speed so that the luminescence time was effectively prolonged to allow a longer measurement time for the IR beam. Our scheme provides a simple and economic means of IR beam inspections, especially useful for the wavelength band above 1,000 nm where the solid-state image sensors are hardly available in low cost.

Keywords Infrared analysis • IR viewing instrument • Beam analysis • IR-sensitive phosphor

2.1 Introduction

Infrared (IR) light is invisible electromagnetic radiation with a wavelength longer than that of visible light. Near-IR radiation of relatively short wavelengths, ranging from 700 nm to 1,700 nm, is particularly of practical interest in applications such as

J. Chang
Hankuk Academy of Foreign Studies, Yongin-si, South Korea

J. Lee · S. Moon (✉)
Kookmin University, Seoul, South Korea
e-mail: moons@kookmin.ac.kr

optical communications, biomedical imaging and optical measurements due to the wide availability of light sources and transparent materials in the near-IR band. It is widely demanded to visualize the near-IR beams in those application fields for testing the basic properties of the IR beam [1–5]. An IR viewer that converts the IR radiation to a visible image of the beam can be used for laser safety or beam characterizations as a routine tool of development and maintenance [2–5]. An IR viewing card is the most popular means for detecting the invisible IR beam in an economic way. The phosphorous screen of the IR viewing card emits visible fluorescence in response to the incident IR radiation and easily visualizes the spatial pattern of the IR beam [2, 3]. Compared to a heavier instrument of an IR viewing scopes which combines an IR camera and a display unit in an instrument [5], the IR viewing card is much cheaper and easier to use for practical IR beam inspections. It has been widely utilized in the near-IR applications when the presence of the IR light needs to be checked with rather qualitative information on the spatial distribution of the light fields. Still, accurate and quantitative beam analysis requires IR-sensitive cameras such as a more expensive InGaAs image sensor for the wavelengths above 1,000 nm.

For IR-responsive luminescence, the screen of the IR viewing card must rely on a multi-photon process. A single IR photon alone cannot produce visible light because of the lower energy of the IR photon. The principle of the IR sensing is far different from ultraviolet-to-visible conversion which is easily achieved by the fluorescence of a partially energy-dissipating process. Two different types multi-photon processes can be used for the purpose of the IR-to-visible conversion in the IR viewing card: up-conversion and light charging. In up-converting phosphor, more than two low-energy photons are absorbed virtually simultaneously by help of the intermediate states [6]. The final high energy is released at once to make a visible photon by fluorescence. The up-conversion IR viewing card is convenient to use but has several disadvantages. It usually has a narrow spectral range of IR detection with a relatively low conversion efficiency. The IR sensitivity is frequently unacceptably low for typical up-converting phosphors when the intensity of the IR is relatively low. The non-proportional response of the nonlinear process also degrades the applicability of this method, which distorts the spatial characteristic of the detected IR beam significantly.

In the IR viewing card based on light-charging phosphor, a visible or ultraviolet photon is absorbed at first to excite the phosphor molecules in a meta-stable state of a very long lifetime [7]. An IR photon that comes after the energy charging triggers the energy release with a visible fluorescence which signifies the IR light. The light-charging IR viewing card, thus, requires a procedure of light charging before being used for the IR detection. Due to the wide wavelength range of a single card and a high sensitivity of the IR detection capability, this type of IR viewing cards are popular in the near-IR applications in spite of the notable inconvenience of light charging requirement. The real drawback of the light charging IR viewing card is found in the nature of *discharging effect*. Because a limited number of molecules are involved in the IR sensing, the excited electrons become depleted by the luminescence process. The card only maintains the luminescence brightness for a short time, typically for a few seconds when exposed to an intense IR beam. Once discharged, its conversion efficiency does not recover unless it is recharged

with intense visible light. Shaking the IR viewing card by the user's hand can help extend the luminescence time but hinders quantitative estimation of the beam characteristic in actual use. After all, the IR viewing card can just provide a limited chance to check the approximate position and the size of the IR beam. A better IR visualizing means is highly demanded for various inspection purposes with capabilities of rather quantitative IR beam analysis.

In this report, we present a new scheme of IR visualization that greatly improves the performance of the light-charging IR viewing card. In our scheme of the rotating IR-sensitive screen, the IR-responsive screen based on the light-charging phosphor is rotated in a high speed to increase the exposure area of the IR beam and, hence, to increase the luminescence time with a reduced local depletion of excited molecules. Despite the simple principle, it effectively allows measurements of the IR beam in a longer time with reduced distortion of the detected spatial pattern. More quantitative analysis of the IR beam is enabled in such a very simple and economic method. We have experimentally tested the feasibility of the IR visualizer based on the rotating IR-sensitive screen and have found that our scheme can provide an inexpensive but effective scheme of IR beam analysis.

2.2 Experiment

In this research, a commercially available IR viewing card that requires visible light charging for IR detection (VRC5, Thorlabs Inc.) was utilized [2]. Figure 2.1 shows the approximate IR detection sensitivity obtained from the manufacturer's datasheet. The intensity of the visible luminescence is plotted as a function of incident IR wavelength. The IR detection range was so wide that a single IR viewing card could cover the whole near-IR band. Once charged by visible light, the phosphor screen could detect the IR light for a long latency time, longer than tens of minutes, and emitted reddish orange light in response to incident IR radiation.

Our IR visualizer was made of an IR-sensitive screen mounted on an electric motor that can rotate the screen stably. The IR detection wheel of a circular plate was prepared so that half of the wheel was covered with the IR-sensitive screen obtained from the commercial IR viewing card (VRC5) while the other half was covered with a non-fluorescent orange plate. The diameter of the wheel was 36 mm in full. A super-luminescent LED was placed above the wheel and could be used for light charging with the intense white light. The screen was uniformly charged before being used by turning the LED on while the wheel was rotating. Figure 2.2 shows our IR visualizer in an experimental setup for testing the feasibility. A collimated IR beam from a fiber-optic light source was launched to the IR detection wheel with an angle of 61° with respect to the plane of the wheel. The wavelength and the beam diameter of the IR beam were 1,310 nm and 2.09 mm, respectively. A digital camera built with a silicon image sensor was used to capture the IR-induced luminescence pattern, which represents the shape of the IR beam projected onto the IR-sensitive screen.

Fig. 2.1 IR-induced luminescence intensity versus wavelength of the incident IR for the IR-sensitive screen used in our experiment [2]

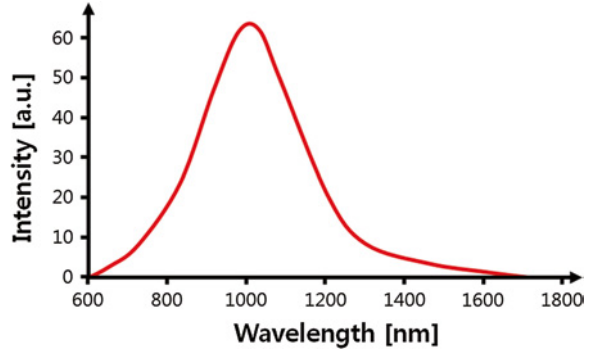
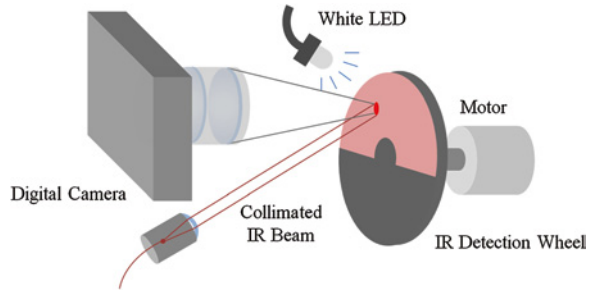


Fig. 2.2 Experimental setup for testing the IR visualizer



After charging the screen, the conversion of IR to visible light was better observed with a higher contrast by turning off the charging light. The principle of our IR visualizer is to increase the effective detection area by rotating the wheel of the IR-sensitive screen. For a point of the screen, the IR exposure time is greatly reduced by such a scanning mechanism. Filling the half of the wheel only with the active phosphorus screen, the visible pattern automatically flickered in a high frequency due to the rotation. It could help the user sense the IR response with better awareness. Flickering luminescence was easily distinguished from ambient light or a visible pattern occasionally incident upon the screen.

A comparative experiment was performed to evaluate the improvement in IR detection made by our scheme compared to an IR viewing card in a fixed position. This was performed for two different cases with the same setup. In the case of the *rotating IR detection wheel*, the electric motor rotated the wheel at a speed of $\sim 1,000$ r.p.m. In the case of the *fixed IR detection wheel*, the wheel was fixed so that the IR beam pointed at a constant position on the active IR-sensitive screen on the wheel. The latter case corresponded to the conventional use of the IR viewing card. For each case, three different intensities of IR rays, 0.55, 1.81 and 5.07 mW for an effective beam area of 0.27 cm^2 , were applied to the IR detection area and were recorded for comparison. Then, the intensity and the beam width of the IR-induced visible pattern were evaluated from captured images of the IR-induced luminescence.

The experiment was carried out in the following steps. For the fixed IR detection wheel, the IR-sensitive screen was charged fully by being exposed to the white light of the LED. The screen was left in dark environment for 30 s after the charging was finished. Next, the IR beam was launched onto the screen while the camera recorded the IR-induced visible pattern that the screen produced. These procedures of charging and IR irradiation were repeated with different IR powers in the same condition and procedures. As well, this experiment was also performed for the rotating IR detection wheel case in the same way. To obtain a wider dynamic range of the measurement, the exposure time of the camera was adjusted in keeping the frame rate at 5 frames/s so that no pixel was saturated. The recorded digital images were processed in a computer to find the intensity of the IR-induced luminescence at the center of the beam. The measured pixel value of luminescence was normalized by the camera's exposure time for each measurement. The change of the relative intensity in time was compared for the different cases. The apparent beam width was also evaluated in full width at half maximum (FWHM) along an axis from the acquired images. And its change in time was also analyzed to find beam measurement errors of the spatial characteristic.

2.3 Result and Discussion

We have analyzed the spatial distributions of the IR-induced visible patterns through the images taken by the digital camera. Its variation in time, t , was evaluated to find the effect of discharging for the two cases. In the description of the experiment results, $t = 0$ was set to be the time of starting the IR irradiation. Figure 2.3 shows the images and contour map representation of the luminescence intensity for the two cases: (a), (b) and (c) for the case of the fixed wheel; (d), (e) and (f) for the case of the rotating wheel. The plots of Fig. 2.3g, h show the intensity distributions along the vertical dotted lines of the contour maps for those two cases, respectively. In detail, Fig. 2.3 shows the image of the acquired visible pattern at $t = 2$ s (a), its contour map representation (b) along with the contour map of the visible intensity at $t = 8$ s (c), respectively. For the rotating case, it also shows the image at $t = 2$ s (d), the intensity-based contour map at $t = 2$ s (e) and $t = 20$ s (f). The inset square in Fig. 2.3a or d gives a scale factor of $1\text{ mm} \times 1\text{ mm}$. Note that the circular IR beam was projected onto the screen with an incidence angle of 29° which resulted in the oval shapes of the visible patterns. As a consequence, the circular cross-section of the beam was slightly extended along the horizontal axis in those images.

The images and contour maps of Fig. 2.3 suggested that the fixed wheel case suffered from the drastic decrease in intensity of the IR-induced luminescence in a few seconds after the IR irradiation started. In addition, the spatial distribution of the IR intensity was incorrectly represented when the discharging effect considerably reduced the visible luminescence. It is easily explained by the fact that the center of the beam experienced the fastest depletion of the excited molecules due to the highest IR intensity. This effect obviously made it difficult to find the center

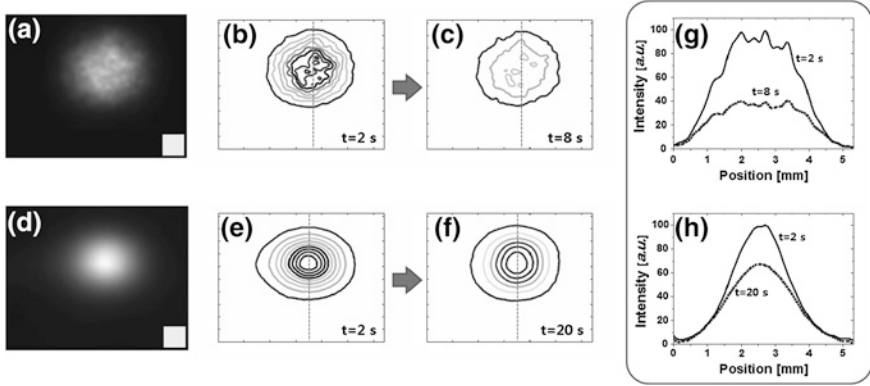


Fig. 2.3 Visible pattern of the IR beam at $t = 2$ s (a), its contour map representation (b), that of the visible intensity at $t = 8$ s (c), respectively, for the case of the fixed IR detection wheel; shown with the visible pattern acquired at $t = 2$ s (d), the intensity contour maps acquired at $t = 2$ s (e) and $t = 20$ s (f) for the case of the rotating IR detection wheel, respectively. The intensity distributions along the *vertical dashed lines* of the contour maps are plotted in (g) and (h)

of the beam and the beam width with the IR viewing card. In contrast, the rotating wheel provided much better representation of the IR beam with reduced discharging effect as clearly observed in Fig. 2.3e, f. One more advantage of the rotating wheel is found in its smooth images. The images of the fixed wheel directly reflected the roughness of the screen surface as seen in Fig. 2.3a. The rotating wheel smoothed the irregularity of the surface by the fast rotation and gave clearer representation of the IR intensity distribution as observed in Fig. 2.3d. The Gaussian-like beam characteristic was successfully measured with our IR visualizer as observed in Fig. 2.3.

The decrease of the IR-induced luminescence at the center of the beam in time was evaluated from the image data. For better precision, the luminescence values of the neighboring pixels in the vicinity of the center were averaged to find the *central intensity*. Figure 2.4 shows the central intensity of the IR-induced luminescence as a function of time, t , for the case of the fixed IR detection wheel (a) and that of the rotating wheel (b), respectively. For the fixed case, discharging effects were clearly observed with the nearly exponentially decaying curves. The luminescence time was defined as the time of luminescence by which the IR-induced luminescence decays to the half of the peak intensity. It was measured to be 2.7 s with an incident IR power of 5.07 mW, 6.1 s with a power of 1.81 mW, and 19.6 s with a power of 0.55 mW. The rotating IR detection wheel also exhibited a decaying characteristic but with a much longer luminescence time. It was measured to be 35 s for the incident IR power of 5.07 mW. It was longer than 80 s when the IR power was less than 1.81 mW. This observation demonstrated our scheme extends the effective measurement time by a factor more than ten compared to the conventional IR viewing card.

Discharging or the decay of the IR-sensitive luminescence does not only decrease the luminescence intensity but also disturbs the accurate measurement of the beam shape and the position determination. The difference in decay speed

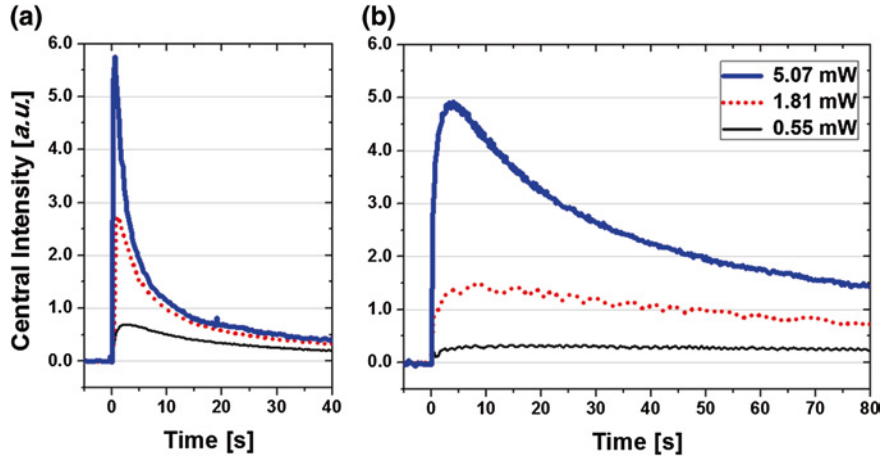


Fig. 2.4 Central intensity of the IR-induced luminescence as a function of time, t , for the case of the fixed IR detection wheel (a) and that of the rotating wheel (b), respectively

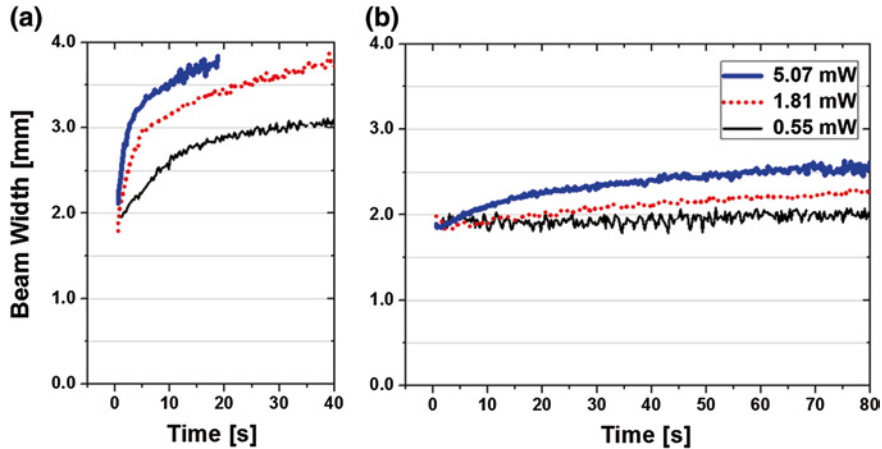


Fig. 2.5 Measured beam width of the IR-induced visible pattern of the fixed wheel case (a) and that of the rotating wheel case (b), evaluated in FWHM, respectively

is explained by the different IR intensity for each position of the screen. As the central region decreases fastest in luminescence intensity, the beam width extends accordingly. From the image data, the beam width was measured long the vertical axis of each image. Figure 2.5 shows the beam width of the IR-induced visible pattern of the fixed wheel case (a) and that of the rotating wheel case (b), measured in FWHM, respectively. Note that the actual beam width of the IR beam was measured to be 2.09 mm. For the case of the fixed IR-sensitive screen, the

measured beam width increased very rapidly as the discharge of the phosphor screen. Even for a low IR power less than 1 mW, it could not be in an acceptable range of error unless the measurement was done in a few seconds after the IR irradiation started. In contrast, the rotating IR-sensitive screen gives much more accurate results within a measurement time of half a minute. It suggested that accuracy and precision could be enhanced by our scheme of the rotating screen with a better representation of the spatial characteristic of the IR beam.

2.4 Conclusion

In this report, we present a low-cost IR beam analysis tool based on a rotating IR-sensitive phosphor screen. The infrared light incident on the IR-sensitive screen was converted to visible light by the phosphor that operated by light charging and IR-induced luminescence. The measurement range of IR wavelength was so wide, from 600 through 1,600 nm, that the entire band of the near-IR region was covered at once. Through comparative experiments were performed to compare our scheme with the conventional IR viewing card based on the same kind of phosphor. It was found that the stationary use of the IR-sensitive screen exhibits a very short luminescence time because the excited fluorescent molecules are depleted locally at the beam spot. This effect was found to hinder accurate estimation on the spatial characteristic of the IR beam. It limits the capability of the IR viewing card in beam inspection. Our IR visualizer alleviates this effect by the rotating IR-sensitive screen in a high speed so that the luminescence time was effectively prolonged to allow a longer measurement time for the IR beam. The experimental result demonstrated that our scheme provides a simple and economic means of IR beam inspections. This new technique of IR beam characterization can be a useful tool of IR inspection for the wavelength band above 1,000 nm where the solid-state image sensors are hardly available in low cost.

References

1. Derickson D (1998) Fiber optic test and measurement. Prentice Hall PTR, New Jersey
2. Laser Viewing Cards, Thorlabs Inc. http://www.thorlabs.com/newgrouppage9.cfm?objectgroup_id=296&pn=VRC5#7125
3. Fonda GR, Schenectady NY (1948) Infrared-responsive phosphors. United States Patent No: 2, 447–322
4. Ebitani M, Tominaga T, Kishi A (1995) Infrared-to-visible converter. United States Patent No: 5, 438–198
5. IR and UV Viewing Scopes, Edmund Optics Inc. <http://www.edmundoptics.com/lasers/laser-measurement/infrared-ir-ultraviolet-uv-viewers/ir-uv-viewing-scopes/1402>
6. Auzel F (2004) Upconversion and anti-stokes processes with f and d ions in solids. Chem Rev 104:139–173
7. Goldstein B, Dropkin JJ (1962) Infrared sensitivity of the ZnS:Cu:Co phosphor. Phys Rev 126:966–970

Progress in Optomechatronic Technologies

Proceedings of the 2013 International Symposium on
Optomechatronic Technologies, Oct 28–30, 2013, Jeju
Island, Korea

Tutsch, R.; Cho, Y.-J.; Wang, W.-C.; Cho, H. (Eds.)

2014, IX, 205 p. 142 illus., 60 illus. in color., Hardcover

ISBN: 978-3-319-05710-1